ACS NANO

www.acsnano.org

ARTICLE

Asymmetric Nanochannel Network-Based Bipolar Ionic Diode for Enhanced Heavy Metal Ion Detection

Jaehyun Kim, Joa Jeon, Cong Wang, Gyu Tae Chang, and Jungyul Park*

Cite This: *ACS Nano* 2022, 16, 8253–8263

Read Online

ACCESS | Metrics & More | Article Recommendations | Supporting Information

ABSTRACT: A higher rectification degree in ionic diodes is required to achieve better performance in applications. Nonetheless, the active geometrical change that is critical for inducing electrical potential asymmetry is difficult to realize in typical ionic diodes because of the intrinsic limitation of the fabrication method. Here, we propose a nanochannel-network-based bipolar diode with a high rectification degree of ∼1600—the highest value realized until now, to the best of our knowledge. Such a high rectification is obtained based on the synergetic effect of the bipolar surface charge and the optimization of the microchannel through experimental studies and multiphysics numerical simulations. It induces ion concentrations at the heterogeneous junction based on the accumulation effect under the forward potential bias. In particular, this proposed molecular concentration occurs in the ohmic region without vortex and instability that is inevitable at the conventional nano-electrokinetic concentration. Combining this accumulation with the horizontally aligned configuration of the nanochannel network membrane (NCNM), a highly sensitive and quantitative mercury ion (Hg^{2+}) sensor based on a fluorescent signal is fabricated that allows direct measurement using a general fluorescent microscope. The detection limit of Hg^{2+} is 10 pM, which is ∼10 times lower than the best detection limit realized so far (∼100 pM) in fluorescent dye-based detection. This demonstrates the potential of asymmetric NCNM for high-performance ion transport in applications such as energy conversion, based on its design and material flexibility.

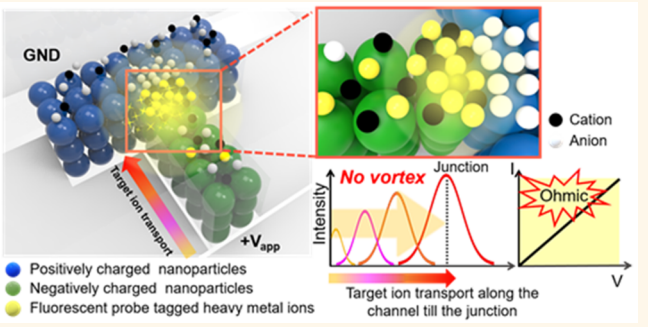

KEYWORDS: *Bipolar ionic diode, Ion current rectification, Ionic junction, Geometrical optimization, Biosensor*

Downloaded via TSINGHUA UNIV on November 4, 2022 at 14:49:24 (UTC).
See https://pubs.acs.org/sharingguidelines for options on how to legitimately share published articles.

Ion transport through artificial nanochannels has been intensively studied in recent decades for mimicking the functions of ion flow in biological ion channels.[1−3] The three main functions of biological ion channels are ionic selectivity, gating, and ionic rectification that are associated with their respective roles in living organisms, for example, energy conversion and sensing.[3] Artificial nanochannels or nanopores are more stable and robust than biological channels and can be practically applied in many domains such as energy harvesting,[4,5] desalination,[6] and biosensing.[7−9] By introducing asymmetric attribution to nanochannels, a nanofluidic ionic diode can be obtained that allows the preferred ionic flow in one direction and the suppressed flow in the other direction.[2] The ionic diodes are the basic elements for mimicking the functions of biological channels and have roles such as separation, sensing, and energy conversion. Ionic diodes are classified into two types, unipolar and bipolar, depending on the charge polarity of the nanochannels. A unipolar diode has only a single-polar charge on the surface of the ionic diode, while a bipolar diode has both positive and negative charges on the surface.[1] Generally, the bipolar ionic diode offers a higher rectification degree than a unipolar ionic diode,[10] and the bipolar ionic diode with asymmetric nanochannel geometry exhibits a higher performance than the bipolar ionic diode with symmetric geometry. However, because the realization of patterning bipolarity in tiny nanochannels is challenging, a bipolar ionic diode with asymmetric nanochannel geometry was proposed in a limited way, such as the track-etched technique with bipolar surface modification.[11,12]

Received: February 26, 2022
Accepted: April 15, 2022
Published: April 20, 2022

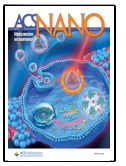

ACS Publications

© 2022 American Chemical Society

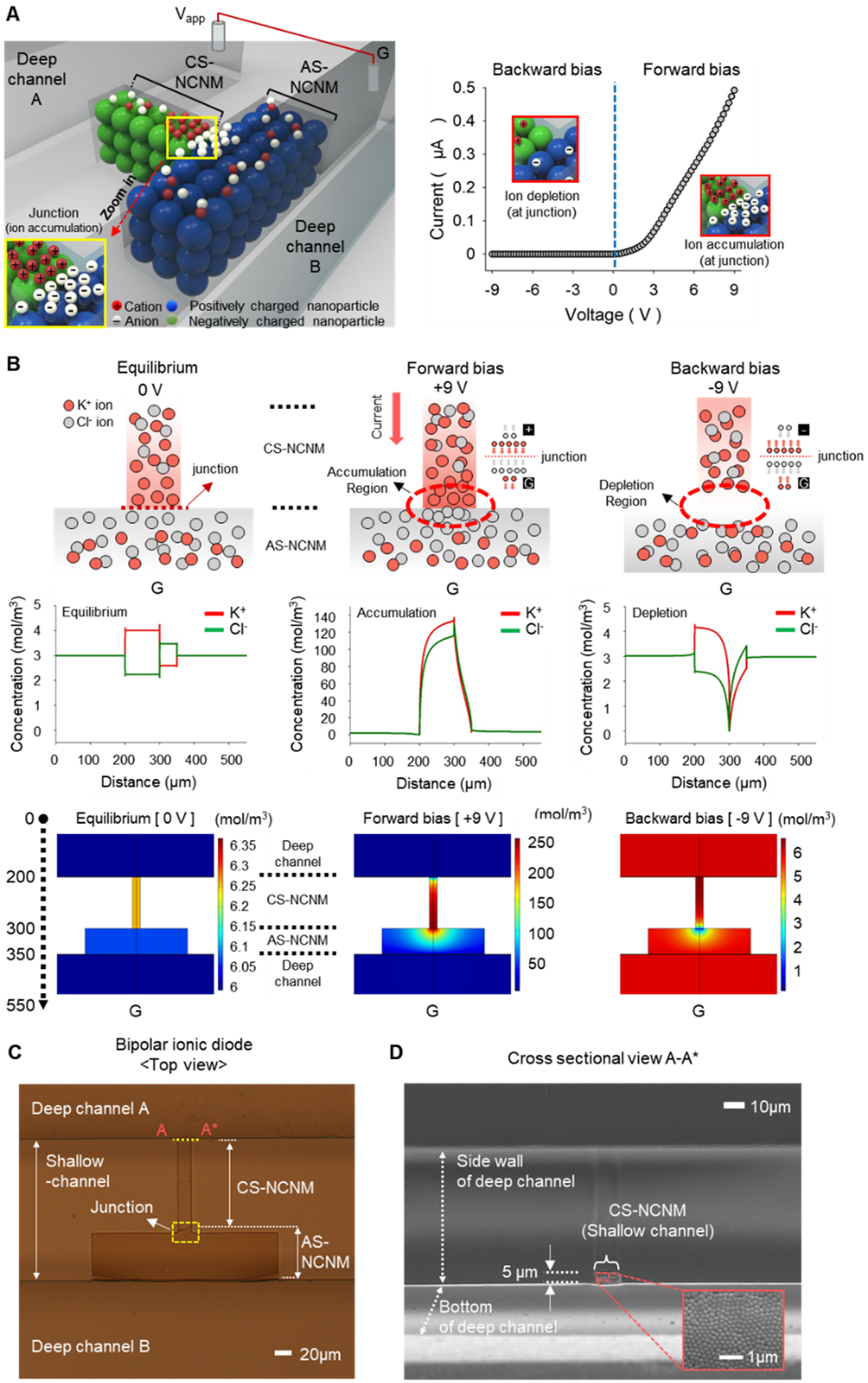

Figure 1. Schematic, working principle, and fabrication results of the proposed bipolar ionic diode. (A) Schematic of asymmetric NCNM-based bipolar ionic diode. (B) Working principle of the bipolar ionic diode that depicts the different ionic distributions depending on the applied potential and the corresponding ionic concentrations calculated via numerical simulation. (C) Microscopic image of the fabricated bipolar ionic diode. (D) SEM image for cross-sectional view of the CS-NCNM filled with nanoparticles (A-A′ section in panel C).

After Martin *et al.* reported an asymmetric unipolar ionic diode,[13] many researchers have developed diodes with various asymmetric geometries including tapered conical,[13,14] funnel-shaped,[12,15] structure-tailorable,[16] and asymmetric branched nanochannels.[17] Compared with these studies, our previously proposed asymmetric nanochannel network membrane

https://doi.org/10.1021/acsnano.2c02016
ACS Nano 2022, 16, 8253−8263

(NCNM) constructed based on self-assembled nanoparticles with homogeneous surface charge[18−22] demonstrated that the ionic rectification can be controlled by the geometrical change of the microchannel that can be adjusted almost freely via standard soft lithography.[21] Before we reported our findings, the unipolar ionic diode was realized based on only asymmetric geometry with nanoscale dimensions comparable to the electrical double layer thickness (EDL). In the case of NCNM, counterion selectivity gradients along the asymmetric NCNM can be induced based on the asymmetric geometry of the microchannel. This causes ion accumulation or depletion within the NCNM under forward and reverse potential biases, resulting in a unidirectional ionic current.

Another advantage of asymmetric NCNM is that ion transport through the nanochannel networks can be observed directly using a fluorescent signal owing to the horizontally aligned configuration that is almost impossible in the other reported fabrication methods for asymmetric ionic diodes. NCNM has several additional advantages, including a high ionic current (∼1000 times higher than the typical conical nanopore), easy fabrication and integration into a microfluidic system, and a wide selection of materials and pore sizes. Specifically, the quantification of the high ionic current owing to 3D NCNM compared with the current of a single nanochannel allows accurate characterization and analysis of ion transport.[23]

This paper proposes a bipolar diode composed of anion-selective NCNM (AS-NCNM) and cation-selective NCNM (CS-NCNM) for the achievement of high rectification degrees based on the synergetic effect resulting from heterogeneous surface charges and the optimal ion selective gradients in asymmetric NCNM determined by the microchannel design. Through experimental investigation of various microchannel designs, nanoparticle sizes, and electrolyte conditions, as well as numerical modeling based on the Poisson−Nernst−Planck equation, the optimal geometrical conditions for the bipolar diode for obtaining a high ionic current rectification (ICR) ratio are obtained, and the proportional relationship between the ICR ratio and ion concentration at the heterogeneous junction of the bipolar diode is confirmed.

On the basis of the high rectification degree, highly sensitive heavy-ion detection is proposed. Previously, the principle of the ionic diode for sensor application was essentially the electrical measurement of the change in the transmembrane ionic current induced by the decrease in the effective cross-sectional area of the nanochannel due to the presence of the analyte[24,25] or by changes in the surface charge due to the binding of target molecules.[26] Our approach is totally different from these previous studies. Our approach is based on fluorescent detection that is possible due to the ionic accumulation and the horizontal configuration of our bipolar ionic diode. The signal can be amplified based on the collection of ions at the heterogeneous junction when a forward bias is applied, similar to that in p-n diodes. While the accumulation of ions at the heterogeneous junction between positive and negative surface charges under forward bias has been studied and modeled theoretically,[27] to the best of our knowledge, the application of sensors based on this physics in the current study has not been attempted before.

RESULTS AND DISCUSSION

Working Principle of NCNM-Based Bipolar Diode. Figure 1A shows a schematic of the proposed NCNM-based bipolar diode with an asymmetric geometric structure and ionic rectification phenomenon under different biases. Owing to the overlapping of EDL between nanopores in NCNM, that is, the nanopore size is comparable with EDL,[28] the bipolar diode exhibits the preferable ion distributions with respect to their surface charge polarity. At the interface between two oppositely charged surfaces, a heterogeneous ionic junction is developed, similar to a p−n junction in a solid-state device. The ions are in the equilibrium state without potential bias: cations are in CS-NCNM and anions in AS-NCNM. When a forward bias is applied, the accumulation zone at which both ions are concentrated is formed at the junction, and high ion transport is induced by the potential gradients along the NCNM. Under the reverse bias, a depletion zone is formed at the junction, and ion transport is suppressed, as shown in Figure 1B.

Monovalent Ionic Distributions in an NCNM-Based Bipolar Diode. The ionic distribution of potassium (K^+) and chlorine (Cl^-) ions in an asymmetric NCNM with respect to the applied potential bias was modeled through finite element analysis (FEA) in COMSOL Multiphysics (Figure 1B). Because the NCNM consists of numerous nanopores between the assembled nanoparticles, the ratio of the nanopore size to EDL thickness ($R = d_n/\lambda_D$, λ_D, and d_n are the EDL and nanopore size, respectively) is an important factor for determining the ion selectivity.[21] The nanopore size is determined to be ∼15% of the diameter of nanoparticles.[29] Here, the simulation for ionic distribution was performed under the conditions of typical experimental environments (KCl 3 mM, $\lambda_{D(AS\text{-}NCNM)} = 6$ nm, $R_{AS\text{-}NCNM} = 5$, $\lambda_{D(CS\text{-}NCNM)} = 6$ nm, $R_{CS\text{-}NCNM} = 3$), and the other detailed conditions including the governing equation for simulation are described in the Materials and Methods and Supporting Information. The obtained graphs and KCl concentration profile as the top view of the 3D model show similar trends in the theoretical results for straight and symmetric bipolar nanochannels reported by Daiguji et al.[27] They show clear accumulation and depletion at the junction under forward and reverse bias, respectively. However, owing to the asymmetric geometry, an asymmetric concentration occurs in each NCNM; in particular, under the forward bias, the ionic concentration increases along the top to bottom of the channel for CS-NCNM gradually and shows a sharp jump-up near the heterogeneous junction, while the concentration decreases rapidly beyond the junction in AS-NCNM (Figure 1B). This confirms that the profile of ionic concentration can be modulated by the geometrical design of the microchannel including the NCNM, and the ICR can be tuned as well.

Figure 1C,D shows the microscopic and SEM images of the proposed bipolar diode fabricated via soft lithography and self-assembly of nanoparticles. The shallow channels were filled with nanoparticles with surface functional groups of $COOH^-$ and NR_3^+ corresponding to CS-NCNM and AS-NCNM, respectively. The cross-sectional view and inset image show the seamless integration of self-assembled nanoparticles in the shallow microchannel, such that tunable ion selectivity is possible in each NCNM.

Geometrical Optimization. In this study, we intend to use the synergetic effects of heterogeneous surface charges and ion selective gradients generated by the shape design of NCNM, to achieve a high ICR. We investigated the variation in ICR according to the change in the geometrical design of

https://doi.org/10.1021/acsnano.2c02016
ACS Nano 2022, 16, 8253−8263

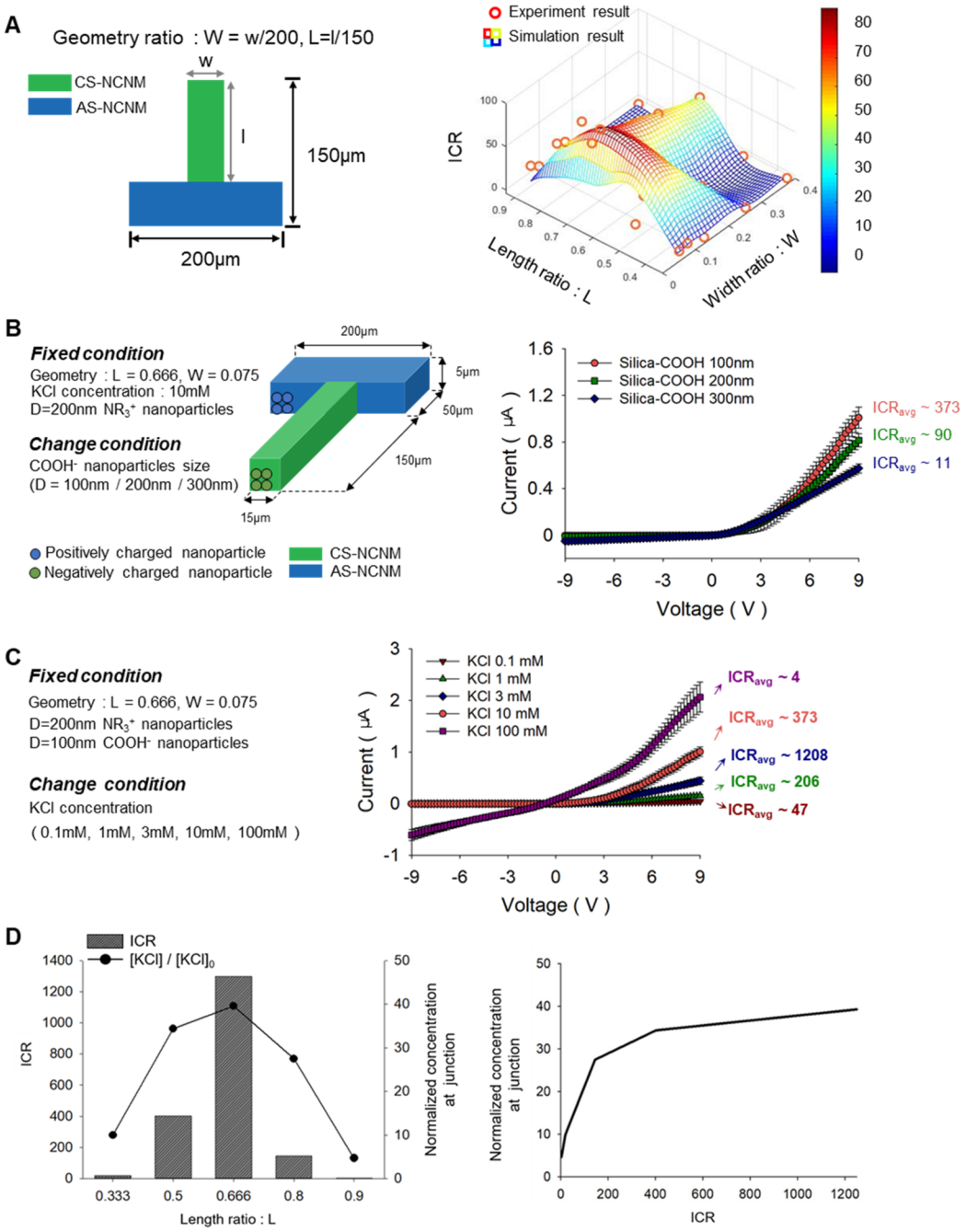

Figure 2. Optimization of the ICR value and relationship between ICR and the concentration at the junction in a single layer device. (A) Standard NCNM design and ICR distribution obtained from experiment and numerical simulation results by changing the area ratio between CS-NCNM and AS-NCNM. *w* and *l* are defined as the width and length of CS-NCNM, and the ratio *W* and *L* are defined as *w*/200 and *l*/150, respectively. (B) Optimization of diameter of nanoparticles with surface functional group $COOH^-$ that forms CS-NCNM, and *I*–*V* curve graphs according to the diameter of nanoparticles (C) Optimization of KCl concentration and its *I*–*V* curve graph. (D) Graphs of the numerical simulation results. Under the conditions of KCl concentration = 3 mM, diameter of NR_3^+ particles = 200 nm, diameter of $COOH^-$ particles = 100 nm, geometry ratio *W* = 0.075, and variable *L*, the relationship between ICR value and normalized ion concentration in the heterogeneous junction is obtained under forward bias.

NCNM in a single layer, the size of the nanoparticles, and the electrolyte conditions.

The standard total length of the NCNM was determined as 150 μm and the width of AS-NCNM as 200 μm, as shown in Figure 2A. CS-NCNM was formed using silica nanoparticles with a diameter of 200 nm and surface functional groups of $COOH^-$ and AS-NCNM using silica nanoparticles with a diameter of 200 nm and surface functional group NR_3^+. ICR values for a total of 25 areal ratios between CS-NCNM and AS-NCNM were investigated by adjusting the width (W) and length ratio (L). Consequently, when the length ratio was ~0.666, that is, when the lengths of CS-NCNM are two times longer than AS-NCNM, the ICR value tended to be high, but when the length ratio was exceedingly high or low, the ICR values were low. Finally, the maximum value of the ICR achieved was ~90 at a width ratio of 0.075 and length ratio of

https://doi.org/10.1021/acsnano.2c02016
ACS Nano 2022, 16, 8253–8263

Table 1. Comparison of Ion Current Rectification Realized Using the Proposed Device with That Reported in Previous Studies

author, [ref] year	material of the device fabrication method	voltage bias	geometry change	maximum average ICR
Zhao et al.,[46] 2020	poly(ethylene terephthalate) (PET)/track etching technique	from −2 to 2 V	difficult	~500
Zhang et al.,[4] 2015	poly(ethylene terephthalate) (PET)/track etching technique	from −2 to 2 V	difficult	~1025
Liu et al.,[47] 2020	anodic aluminum oxide (AAO)/anodization	from −2 to 2 V	difficult	~450
Li et al.,[9] 2019	polycarbonate (PC)/track etching technique	from −1 to 1 V	difficult	~450
Liu et al.,[48] 2020	polyacrylic acid (PAA)/anodization	from −1 to 1 V	difficult	~410
our study	polydimethylsiloxane (PDMS)/soft lithography	from −9 to 9 V	easy	~1208

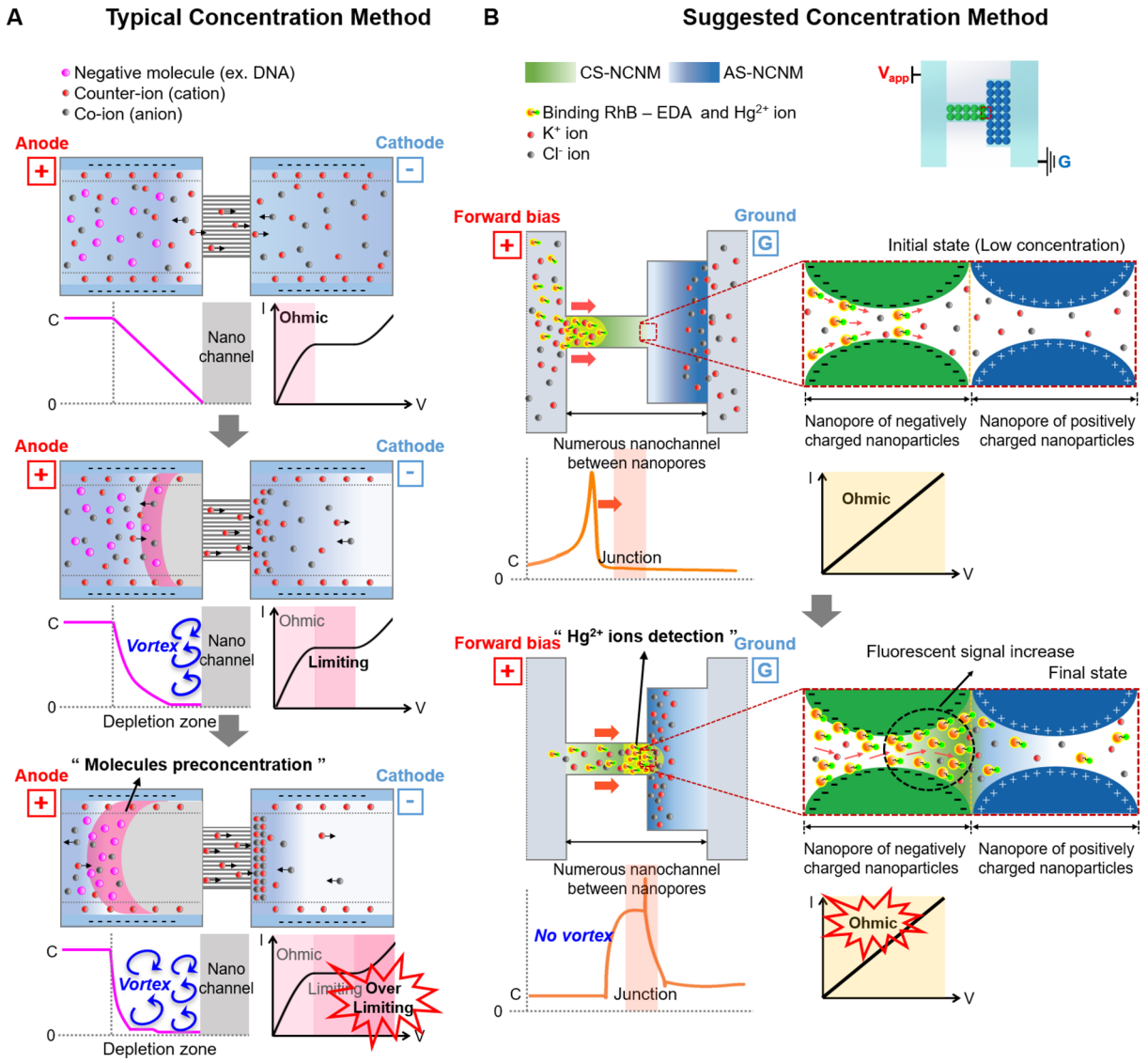

Figure 3. Schematics of the concentration method for micro-/nanofluidic systems based on ion concentration polarization (ICP). (A) Typical concentration method: working principle of molecular preconcentration and concentration profile in the ohmic, limiting, and over limiting regimes. (B) Suggested concentration method: working principle of mercury ion detection and concentration profile in the ohmic regime.

0.666. In addition, we obtained ICR distributions through numerical simulation at a specific geometry ratio (W: 0.05−0.125, L: 0.500−0.800) that were similar to the experimental results, as shown in Figure 2A. The simulation results also have the maximum ICR value at W = 0.075, L = 0.666. Furthermore, to secure a higher ICR, the ion selectivity of NCNMs is expected to be important, and the experiment was conducted by adjusting the particle size (nanopore size) associated with the overlap of the EDL and the ion selectivity. Nanoparticles with sizes of 100, 200, and 300 nm for CS-NCNM, and 200 nm nanoparticles for AS-NCNM were considered for the microchannel design determined as discussed above and 10 mM KCl. When CS-NCNM was formed with 300 nm particles, its nanopore size was 45 nm ($\sim R_{AS\text{-}NCNM}$ = 10, $\sim R_{CS\text{-}NCNM}$ = 15) that was larger than that of the 200 nm particles ($R_{AS\text{-}NCNM}$ = 10, $R_{CS\text{-}NCNM}$ = 10). Therefore, the ion selectivity and ionic current of CS-NCNM with 300 nm particles are lower than those with 200 nm

https://doi.org/10.1021/acsnano.2c02016
ACS Nano 2022, 16, 8253−8263

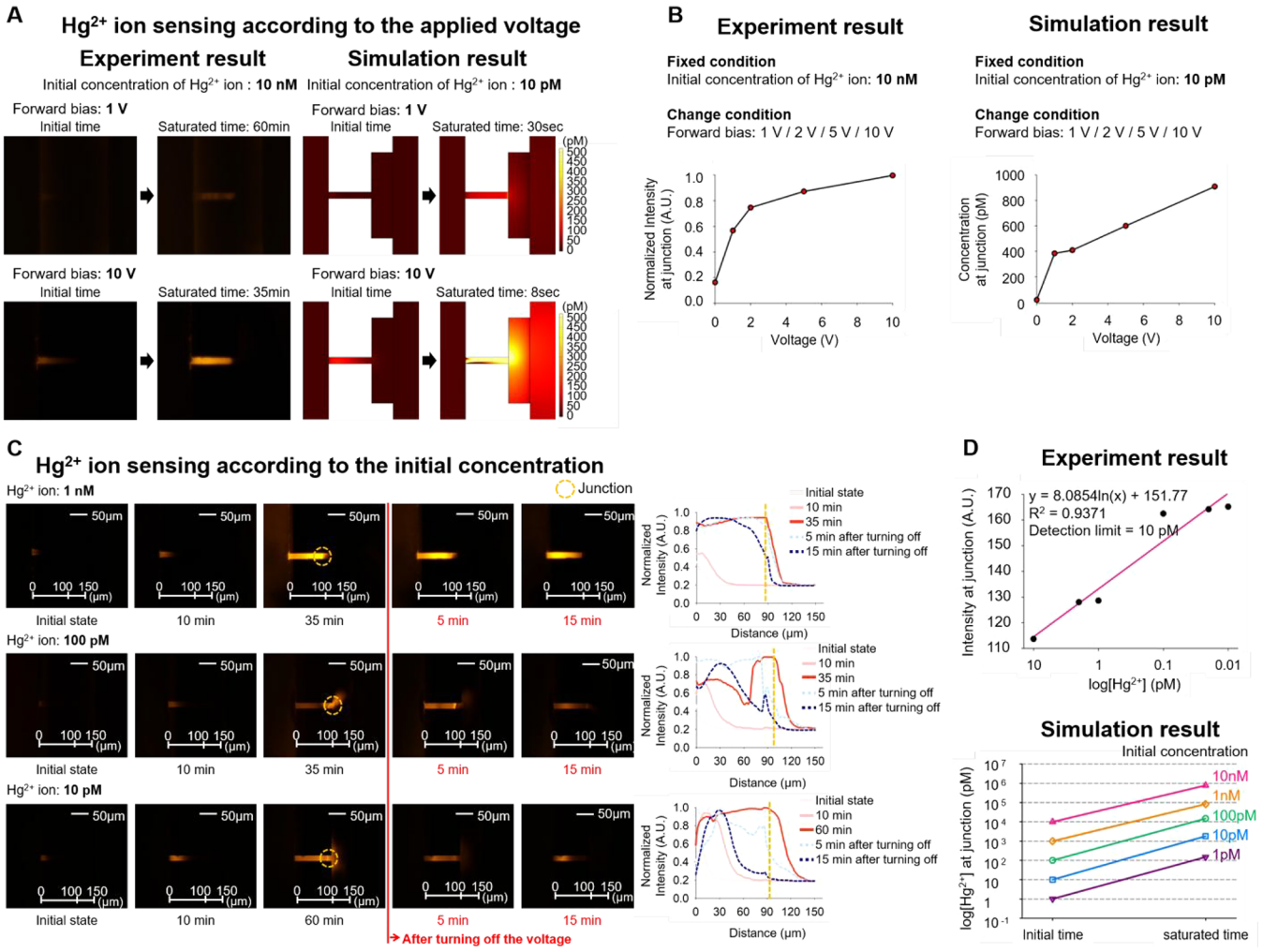

Figure 4. Mercury ion sensing (A) fluorescence images of the NCNM obtained via experimentation and concentration images of the NCNM obtained via numerical simulation according to the applied voltages. (B) The relationship between normalized fluorescent intensity in the saturated state at the junction and the applied voltage (experiment result graph) and the relationship between concentration in the saturated state at the junction and the applied voltage (simulation result graph). (C) Fluorescence images of the NCNM and the fluorescent intensity graph along the microchannel (from 0 to 150 μm). (D) Graph of maximum fluorescent intensity at the junction according to various initial concentrations on the log scale and the graph of the maximum concentration on the log scale at the junction over time for each initial concentration, obtained via simulation.

particles, as the factor R is increased that also induces a low ICR value. Furthermore, when CS-NCNM was formed with 100 nm particles, the nanopore size was 15 nm ($R_{AS\text{-}NCNM}$ = 10, $R_{CS\text{-}NCNM}$ = 5), and subsequently, more overlapping EDL resulted in a higher ion selectivity and higher ionic current. Accordingly, a higher ICR value of 373 could be achieved that is approximately six times higher than that of the 200 nm nanoparticles (Figure 2B). The tendency that smaller nanoparticles produce a higher ionic current (higher conductance) is consistent with our previous work.[21] The factor $R = d_n/\lambda_D$ is also affected by the EDL thickness associated with the ionic concentration of the medium. Therefore, we conducted an experiment to increase the ICR by adjusting the concentration of KCl to 0.1, 1, 3, 10, and 100 mM. In this experiment, as the fixed experimental conditions, 200 nm NR_3^+ functionalized and 100 nm $COOH^-$ functionalized nanoparticles and W = 0.075 and L = 0.666 geometric ratio of NCNM were used. When the KCl concentration was 100 mM, the ion selectivity collapsed because the EDL thickness decreased that reduced the rectification degree, ICR. However, an excessively low ionic concentration (<1 mM) implies a small number of ions in the medium, such that the ionic current decreases. Finally, we obtained the maximum ICR ≈ 1600 (average ICR value = 1208) at 3 mM KCl; this is the highest value to the best of our knowledge. Table 1 shows a comparison of the ICR values obtained in the current study and those obtained in previous studies.

The proportional relationship between the ICR values and the ion concentration at the junction under the forward bias is observed through numerical simulation, as shown in Figure 2D, such that the optimized design with the highest ICR is used for biosensors in the other section.

Detection of Heavy Ions Based on Accumulation Phenomenon. In this paper, we propose the highly sensitive and quantitative detection of heavy metal ions (Hg^{2+}) in a fluid using a bipolar ionic diode with a high rectification degree. This approach is based on the ionic concentration phenomenon at the heterogeneous junction under a forward bias, as shown in Figure 1B. This suggested concentration method realizes a vortex-free stable ionic concentration in the ohmic

https://doi.org/10.1021/acsnano.2c02016
ACS Nano 2022, 16, 8253−8263

region that is different from the typical nano-electrokinetic concentration method. Figure 3 compares the concentration principles between the suggested and typical concentration method.[30−32] The typical concentration method uses the principle of ion concentration polarization (ICP) based on the asymmetric ion transport of cation and anion as shown in Figure 3A. When a potential is applied to the microdevice with ion-selective nanochannels, the counterion can pass through the nanochannels only. Then, an enrichment (cathode side) and a depletion zone (anode side) occur at each interface of micro- and nanochannels for maintaining electrical neutrality. Because of the balance between electrophoretic migration (EP) and electroosmotic flow (EOF), the preconcentration is induced at the depletion boundary on the anode side.[33] The depletion effect does not appear in the ohmic region. After that, the depletion zone is formed in the limit current regime associated with the limited ion transport through the depletion zone. When the voltage increases beyond the limit current regime, the current is further increased, known as the overlimiting region. At this time, the ions and molecules are pushed outside of the depletion zone by strong and fast vortex flows, and the preconcentrated region is formed. This preconcentration has already been used for biomolecular detection in previous studies owing to the enormous fluorescent signal amplification. Nonetheless, owing to the vigorous vortex, the additional pressure field should be applied to control the preconcentrating plugs stably.[32] However, the preconcentrating plug loses its stability over time,[34] and therefore, stable and quantitative sample analysis is limited in the typical method.

Conversely, the suggested concentration method enables the realization of a stable concentration plug without vortex flow, as shown in Figure 3B. We used the optimized bipolar diode device as a fluorescence-based sensor because it is expected that a higher rectification degree, ICR, can induce a higher concentration, as shown in Figure 2D. First, the positively charged target ion with fluorescent probes is injected into the deep channel in the CS-NCNM direction. When a forward bias is applied, the target ions, along with the existing cations and anions, continuously migrate and accumulate at the entrance of the CS-NCNM owing to the electric drift forces and diffusion and the convection flow. Over time, the target ions continue to move through numerous nanochannel networks between the nanopores, and many migrated target ions accumulate near the heterogeneous junction between CS-NCNM and AS-NCNM. Consequently, the fluorescent signal increases significantly, and highly sensitive direct sensing is possible via general fluorescent microscopy. Unlike the typical concentration method, the suggested concentration method enables stable and quantitative detection in the nanochannel network membrane without vortex flow by applying relatively low potential within the ohmic region. The ohmic behavior of the proposed device can be confirmed by the experimental data shown in Figure 2.

To confirm the proposed sensing mechanism, the detection of Hg^{2+} ions was conducted through experimental and simulation studies. To demonstrate the stable ion sensing in the ohmic region, we conducted the experiment according to the applied voltage from low potential and confirmed its behavior through simulation. In the experiment, the initial concentration of Hg^{2+} ions was fixed at 10 nM, and the experiment was performed at voltages of 1, 2, 5, and 10 V in the ohmic region. The left side in Figure 4A shows the images acquired at the initial time and the time to saturation with voltages of 1 and 10 V at an initial concentration of 10 nM. (Experimental data and CCD images acquired with other voltages are shown in Supplementary Figure S6.) We performed CCD imaging based on an exposure time of 100 ms. The Hg^{2+} ion solution was continuously injected at a flow rate of 50 μL/min using a syringe pump. At a low voltage (1 V), the fluorescence intensity is relatively small, and the time to saturation is relatively long; at a high voltage (10 V), relatively high intensity is obtained in the short saturation time. The right side in Figure 4A shows the concentration distributions obtained by the simulation at the initial time and the time to saturation with voltages of 1 and 10 V and an initial concentration of 10 pM. The simulation results also show similar ion concentration behavior for Hg^{2+} ions at the junction when two different potentials are applied. In experiments, because the target Hg^{2+} ions are tagged by fluorescent probes, the diffusivity of the combined molecules is much lower than that of pure Hg^{2+}. Therefore, the time to saturation in the experiments is longer than that in the simulations. Quantitative sensing according to the applied potential was verified, as shown in Figure 4B. The left side shows the normalized intensity graph according to the voltage (0−10 V), when the intensity is saturated at the junction, in the experimental results. The right side is the concentration graph according to the voltage (0−10 V), when the concentration is saturated at the junction, in the simulation results. In both experiments and simulations, the detected signal (fluorescence intensity and Hg^{2+} concentration) is linearly proportional to the applied potential. When 10 V is applied, concentration amplification of ∼100 times is possible in the simulation results; that is, the initial concentration of 10 pM increases to ∼1000 pM.

Figure 4C shows the experimental results of Hg^{2+} ion sensing at various initial concentrations. These data are the experimental results for the initial concentrations of 1 nM, 100 pM, and 10 pM, and the additional data on the experimental results for other initial concentrations are shown in Supplementary Figure S7. We observed the ion detection process over time, and the graphs of the normalized fluorescence intensity along the NCNM were obtained from the CCD images via a simple imaging process. A 20 V forward bias was applied to achieve a higher fluorescence intensity and faster time to saturation. The medium containing Hg^{2+} ions at various concentrations was continuously injected at a flow rate of 50 μL/min. When the images and graph for each concentration were checked, the concentrated plugs observed at the entrance of CS-NCNM migrated from left to right over time, and their fluorescent signal increased significantly near the junction (100-μm position) after more than 30 min. A lower initial concentration required a longer time to saturation. Additionally, the concentrated ion movements after turning off the applied voltage were observed. When the voltage is turned off, the amplified fluorescence intensity near the junction decreases, and the concentrated plug retreats slowly from the junction over time by diffusion (Figures 4C and S5B). Obviously, since the Hg^{2+} ions cannot move over the junction, the diffusion occurs one way toward the entrance of CS-NCNM. The calibration graph on the top in Figure 4D shows a linear relationship between the maximum fluorescent intensity at the junction and the initial ion concentration on the log scale. The high rectification degree obtained by geometrical optimization controls ion transport with high performance and increases the ion accumulation at the

https://doi.org/10.1021/acsnano.2c02016
ACS Nano 2022, 16, 8253−8263

heterogeneous junction. This results in a detection limit of 10 pM that is ∼10 times lower than the best value (∼100 pM) obtained so far in fluorescent organic dye-based detection.[35,36] The graph on the bottom in Figure 4D shows the simulation results of the accumulated Hg^{2+} ions at the junction with respect to the initial concentrations (from 1 pM to 10 nM) on a log scale. Consequently, it indicates that the saturated concentration at the junction is increased by ∼100 times relative to the initial concentration that is almost independent of the initial concentration. The concentration distributions and profiles for Hg^{2+} ions obtained by numerical simulation are shown in Figure S8. Compared to monovalent ions (K^+ and Cl^-), the divalent Hg^{2+} ion is accumulated more, considering its initial concentration. That is a reasonable result seeing Poisson−Nernst−Planck equation owing to higher ion valence (eqs 1−3). The Hg^{2+} ion concentration graph shows a shape similar to the KCl concentration graph at the steady state without convection flow (Figure S8A). If the solution is over the critical concentration (∼1 mM for Mg^{2+}, ∼20 mM for Ca^{2+}), in the multivalent ion transport, the charge inversion happens due to the strongly correlated liquid (SCL) layer, in which the Poisson−Boltzmann equation is no longer valid.[37,38] However, since very low concentrations of divalent Hg^{2+} ion (10 pM to 10 nM) are explored in this study, we ignored the charge inversion in numerical analysis.

The concentration profile for Hg^{2+} can be changed in the CE-NCNM according to the convection flow induced by injection of the ionic solution (Figure S8B). To investigate the degree of influence by the convection flow, the concentration distributions were calculated at the steady state without convection and the time-dependent analysis considering the convection flow (1−50 μL/min). As the flow rate increased, the concentration at the junction increased, and the time to reach saturation decreased. At the flow rate of 1 μL/min, the concentration at the junction reached by ∼80 times the initial concentration, which is almost similar to the result without convection flow (Figure S8A). At a 50 μL/min flow rate, the concentration increased ∼30% more compared to the no convection flow condition. The convection flow effect is further investigated by the experimental study as shown in Figure S9, which shows fluorescent images and the extracted concentration graphs with respect to 2 and 5 μL/min flow rates under 20 V applied voltage and 100 pM initial condition. At these relatively lower flow rates, the fluorescence intensity is relatively low, and the time to reach the saturation is relatively long, but still, it is clearly observable that the Hg^{2+} ions are detected near the junction.

The proposed sensing approach based on the molecular concentration and the horizontally aligned configuration of NCNM presents a stable, quantitative, and highly sensitive detection performance, as expected. The detection through nanochannel networks naturally induces filtration of samples such that the raw sample would be applicable without preprocessing. The application of ion sensors using ion accumulation under forwarding bias could be extended further by considering other metal ions associated with toxicity and health conditions, for example, Cd^{2+}, Pb^{2+}, and Fe^{2+}. Additionally, the numerical simulation can be studied in detail by incorporating physical phenomena that have not been considered yet (adsorption chromatography effect[39]).

CONCLUSION

The convenient and precise structural manipulation and surface modification of ionic diodes is the key to controlling ion transport at the nanoscale. Although various types of ionic diodes have been reported, there are intrinsic difficulties in the fabrication of nanochannels, functionalization with different polarities inside the nanochannel, and change in the geometry, pertaining to the realization of a high degree of ICR. In this study, we propose a bipolar ionic diode fabricated by the self-assembly of nanoparticles with different surface functional groups that are packed in controlled microchannel geometries. The rectification degree was optimized through experimental and simulation studies by regulating various parameters (channel geometry, size of nanoparticles, and medium concentration), and finally, a high rectification degree (∼1600) was achieved. On the basis of the horizontal channel configuration and a strong accumulation effect at the junction of the bipolar ionic diode under forward bias, a stable, quantitative, and highly sensitive fluorescent-based biosensor was proposed, which has a totally different principle from the previous ionic diode-based sensor. Additionally, the proposed concentration mechanism can address the problems in the typical nano-electrokinetic concentration, such as unstable vortex flow, and relatively high applied voltage beyond the ohmic region. The sensitive detection performance for very low concentrated heavy metal ion (10 pM, the lowest detection limit using fluorescent organic dyes for Hg^{2+}, so far) was demonstrated with this mechanism. In the near future, by extending nanoparticle materials with various intelligent functions and through an in-depth understanding of the underlying physics in the proposed bipolar diode, smart ionic devices with multifunctions will be fabricated for various applications such as gating, energy conversion and harvesting, biosensing, and nervous system biomimicking.

MATERIALS AND METHODS

Fabrication of Bipolar Ionic Diode. The proposed bipolar ionic diodes were fabricated via the standard soft-lithography process, as shown in Supplementary Figure S1. A Si wafer was spin-coated with a negative photoresist (SU-8 2005; Microchem Co., USA) and subsequently soft-baked. After the photoresist was exposed for patterning 5-μm height-shallow channels using a mask aligner to ultraviolet (UV) light, the photoresist-coated wafer was placed on a hot plate for hard baking. The mold for shallow channels was formed by removing the unexposed photoresist using the SU-8 developer solution. Another photoresist (SU-8 3050; Microchem Co.) was spin-coated on the patterned mold to form 100-μm deep channels and exposed to UV light, and subsequently, the exposed wafer was hard-baked. Finally, a master mold was fabricated. The surface of the master mold was treated with trichloro(3,3,3-trifluoropropyl)silane (452807; Sigma-Aldrich, USA). After the polydimethylsiloxane (PDMS; Sylgard; Dow Corning Korea Ltd., Korea) mortar was prepared by mixing the curing agent with a volume ratio of 10:1, the mortar was placed in a vacuum jar for degassing for 30 min. The PDMS mortar was poured on a patterned mold and cured at 95 °C for 1 h, after which the cured PDMS was demolded. A microfluidic device was fabricated by bonding the PDMS with a slide glass that was treated with O_2 plasma (Cute-MP; Femto Science, Korea).

NCNMs with positive and negative surface charges were fabricated by the self-assembly of nanoparticles with surface functional groups NR_3^+ (Micromod, Germany) and $COOH^-$ (Micromod, Germany) into the desired regions in the microchannels, as shown in Supplementary Figure S2. By using different sizes of nanoparticles, the pore sizes formed in the NCNM could be easily controlled to investigate the optimized rectification degree in the proposed bipolar

https://doi.org/10.1021/acsnano.2c02016
ACS Nano 2022, 16, 8253−8263

ionic diode. First, the suspension containing NR_3^+ nanoparticles dispersed in 50% ethanol in distilled (DI) water was injected into the reservoir connected to deep channel A. The mixed suspension was introduced into the shallow channel through capillary flow, but it did not pass through the interface of the shallow and deep channel B owing to the neck pressure.[40] Thereafter, the solvent from the suspension was evaporated such that the nanoparticles were drawn toward the interfaces (that is, evaporation-driven self-assembly). When the AS-NCNM is filled with positively charged nanoparticles, the suspension was completely removed from the channel by injecting DI water. Since the evaporation-driven self-assembly became slow at the interface of two compartments of shallow channel compared to the initial assembly at the interface of shallow and deep channels, the desired assembled area could be secured. Subsequently, the suspension containing $COOH^-$ nanoparticles dispersed in 50% ethanol in DI water was injected into deep channel A, and the evaporation-driven self-assembly occurred at the edge of AS-NCNM. After the desired volume of CS-NCNM in the shallow channel was realized, the suspension was completely removed from the channel, and the fabricated device was dried overnight. Supplementary Figure S3 shows the $I-V$ experimental results including the variation of the device-to-device to verify that the similar device can be obtained through the suggested fabrication procedures. The average standard error was ~0.0718 μA for seven samples, which reflected the areas for each polarized region were properly regulated.

Ion Current Measurement. Prior to the ionic current measurement, the nanopores of NCNM were cleaned with 70% ethanol and DI water three times. Following this, KCL with the target concentration was injected, and we waited ~20 min until the equilibrium state was reached. The potential was applied between two deep channels from −9 to 9 V for 0.2 V per 1 s, and the corresponding current was measured. The electrodes were selected as the platinum wire, and a picometer (6487, Keithley) was used to apply the voltage and read current.

Binding of RhB-EDA and Hg^{2+} Ion. We used fluorescent probes (rhodamine B) lactam-1,2-ethylenediamine (RhB-EDA) to observe the quantitative behavior of Hg^{2+} ions in the NCNM of the device.[41] The RhB-EDA, a rhodamine B-based fluorescent probe obtained from Angene International Limited (Hong Kong), a phosphate buffer stock (PBS) solution (Sigma-Aldrich, Korea), and mercury(II) chloride (Sigma-Aldrich, Korea) were used for binding. First, RhB-EDA was diluted in DMSO to prepare a RhB-EDA stock solution. Next, Hg^{2+} was diluted to prepare a stock solution. A RhB-EDA stock solution was mixed with Hg^{2+} stock solution, PBS, and distilled water in a molar ratio of 3:3:14:10.[41] It was studied after being incubated for 20 min at room temperature in the dark. Supplementary Figure S5A compares the image of the RhB-EDA solution before binding to Hg^{2+} ions and the image of the solution in which the fluorescence signal is amplified by combining Hg^{2+} ions with RhB-EDA. The final solution was diluted to the molar concentration required for the experiments. RhB-EDA transforms the spirolactam form with low fluorescence into an open-ring amide with high fluorescence in the presence of Hg^{2+} ions. Thus, the transport of Hg^{2+} ions attached to RhB-EDA can be visually observed as a fluorescent signal in the NCNM covered with transparent PDMS material.

Hg^{2+} Measurement. As shown in Figure 2D, the ion concentration at the junction of the bipolar ionic diode is proportional to the rectification degree (ICR). Therefore, for the measurement and analysis of Hg^{2+}, we used an ionic diode with an optimized geometry ratio (length ratio 0.666, width ratio 0.075) and 200 nm-diameter NR^{3+} nanoparticles in AS-NCNM and 100 nm-diameter $COOH^-$ nanoparticles in CS-NCNM, exhibiting the highest rectification degree.

First, we washed the channel three times with 70% ethanol and three times with DI water, added a small concentration of KCl solution, and waited for it to stabilize. Next, a higher concentration of 3 mM KCl solution was added to facilitate transportation with an extremely low concentration of Hg^{2+} ions. The ionic diode device was connected with tygon tubing to a syringe pump that was responsible for the continuous injection of Hg^{2+} ions into the deep channel.

In addition, the device was connected to a source meter (2400, Kelthley, USA) that provided the potential bias. Deep channel A in the CS-NCNM direction was connected to the forward bias voltage, and deep channel B in the AS-NCNM direction was connected to the ground. The device was subsequently fixed on a fluorescence microscope (Olympus IX71, Japan) with an attached CCD camera. Hg^{2+} ions were injected continuously with various flow rates (2 μL/min, 5 μL/min and 50 μL/min), and 1−20 V forward bias was applied according to the experimental conditions. The migration and accumulation of Hg^{2+} ions were monitored over time using the CCD camera based on the fluorescence intensity.

Numerical Modeling. The bipolar ionic diode was modeled in three dimensions through a finite element method (COMSOL Multiphysics 5.6) for the calculation of the ion concentration distribution and the ion current according to the geometric-ratio change and the applied potential, and for the determination of the relationship. The main modeling system is ion transport under the electric field. It can be solved using two modules: "Transport of Diluted Species (Nernst−Planck equation)" and "Electrostatics (Poisson's equation)".[21,42,43] Additionally, in solving the model related to mercury (Hg^{2+}) ion sensing, the "Laminar flow (Navier−Stokes)" module is used to consider the convection flow.

The transport of potassium (K^+) and chlorine (Cl^-) ions through the asymmetric NCNM at steady state was calculated using the Poisson−Nernst−Planck equation. The conservative equation for ion flux and the Poisson equation are defined as follows:

$$\frac{\partial c_i}{\partial t} = -\nabla \cdot J_i \tag{1}$$

$$\nabla^2 \varphi = -\frac{\rho_v}{\varepsilon_0 \varepsilon_r} = -\frac{F}{\varepsilon_0 \varepsilon_r} \sum z_i c_i \tag{2}$$

where φ is the electric potential, ρ_v is the space charge density; F is Faraday constant, ε_0 and ε_r are the permittivity of vacuum and dielectric constant of the electrolyte solution, and z_i and c_i are the ion valence and concentration of ion species i, respectively. Ion species i are either cations or anions.

The ion flux J_i is given as follows:

$$J_i = uc_i + D_i\left(\nabla c_i + \frac{Fz_i c_i}{RT}\nabla\varphi\right) \tag{3}$$

Here, u is the flow velocity, D_i is the ion diffusion coefficient of ion species i, R is gas universal constant, and T is temperature of the solution, respectively.

In this model, eq 3 is expressed considering the flux induced by hydrodynamic convection, diffusion, and migration under an electric field. The convection flow is ignored for the optimization of geometry based on the concentration distribution of monovalent ions, while it is included for simulating heavy metal detection.

The continuity equation and the Navier−Stokes equations are as follows:

$$\nabla \cdot u = 0 \tag{4}$$

$$\rho\left(\frac{\partial u}{\partial t} + u \cdot \nabla u\right) = -\nabla p + \mu \nabla^2 u + F \sum z_i c_i E \tag{5}$$

where ρ (= 1000 kg/m^3) is the density, μ (= 0.89 mPa·s) is the viscosity of water, p is the pressure, and E is the electric field, respectively.

The geometry of the model was designed with three-dimensional axisymmetric microsized blocks or two-dimensional microsized rectangles, including the deep channel with the same volume as the experimental device and the shallow channel heterogeneously combined with AS-NCNM and CS-NCNM. The detailed simulation models and their boundary and input parameters in NCNM can be referred to in Supplementary Methods, Table S1, and Figure S4 in Supporting Information.

The space charge density in the deep channel ρ_{deep} is calculated using eq 6 according to eq 3.[44] The concentrations of cations and

https://doi.org/10.1021/acsnano.2c02016
ACS Nano 2022, 16, 8253−8263

anions are c_{cat} and c_{an}, respectively, and the charge numbers of cations and anions are z_{cat} and z_{an}, respectively.

$$\rho_{deep} = F(z_{cat}c_{cat} + z_{an}c_{an}) \quad (6)$$

The space charge density in the shallow channel $\rho_{shallow}$ is calculated using eq 7 with the $z_{mem}c_{mem}$ term as an assumption for the membrane on which polar silica particles are arranged.

$$\rho_{shallow} = F(z_{cat}c_{cat} + z_{an}c_{an} + z_{mem}c_{mem}) \quad (7)$$

Here, the concentration of the membrane c_{mem} is calculated by adding $\sigma = \pm 0.01$ C/m^2 that is the surface charge density of silica nanoparticles,[21,45] and $n = 3/4 \times 0.74 \times V/(\pi r^3)$, which is the total number of nanoparticles in NCNM:[21]

$$c_{mem} = \frac{4\pi r^2 n\sigma}{eN_A(1 - 0.74)V} \quad (8)$$

where e, N_A, and r are the charge of the electron, Avogadro's number, and radian of the nanoparticle, respectively. The constant 0.74 is the space occupation rate for the FCC structure in the NCNM.

A simulation was conducted to determine the equilibrium, accumulation, and depletion states of ions in the heterogeneous ionic junction of the model and the calculation of ion current rectification according to the ion current. The ion current (I) is given as the integral of the ion fluxes for cations (J_{cat}) and anions (J_{an}):[43,44]

$$I = F\iint (z_{cat}J_{cat} + z_{an}J_{an})\cdot\hat{n}\, dS \quad (9)$$

where $\hat{n}$ is the normal vector of surface S.

ASSOCIATED CONTENT

Supporting Information

The Supporting Information is available free of charge at https://pubs.acs.org/doi/10.1021/acsnano.2c02016.

Numerical simulation condition, diffusion coefficients of ions in NCNM, information for nanoparticles, soft-lithography process for microfluidic device, spatially controlled self-assembly of nanoparticles for CS-NCNM and AS-NCNM, I–V experimental data showing the device-to-device variation, numerical simulation models, images of RhB-EDA and RhB-EDA-mercury ions, time-normalized intensity curve for mercury ion sensing, fluorescent images and graphs of mercury ion sensing according to the applied voltage and initial concentration, simulated concentration distribution for mercury ions with or without convection flow (PDF)

AUTHOR INFORMATION

Corresponding Author

Jungyul Park − *Department of Mechanical Engineering, Sogang University, Mapo-gu, Seoul 04107, Republic of Korea; Interdisciplinary Program of Integrated Biotechnology, Sogang University, Mapo-gu, Seoul 04107, Republic of Korea;* orcid.org/0000-0002-6885-9466; Email: sortpark@sogang.ac.kr

Authors

Jaehyun Kim − *Department of Mechanical Engineering, Sogang University, Mapo-gu, Seoul 04107, Republic of Korea*

Joa Jeon − *Department of Mechanical Engineering, Sogang University, Mapo-gu, Seoul 04107, Republic of Korea*

Cong Wang − *Critical Analytics for Manufacturing Personalized-Medicine (CAMP), Singapore-MIT Alliance for Research and Technology (SMART) Centre, Singapore 138602, Singapore;* Present Address: School of Mechanical Engineering and Electronic Information, China University of Geosciences (Wuhan), 388 Lumo Road, Wuhan 430074, China; orcid.org/0000-0001-7245-5109

Gyu Tae Chang − *Samsung Electronics Co., Ltd. Samsung-ro, Suwon-si, Gyeonggi-do 16677, Republic of Korea*

Complete contact information is available at: https://pubs.acs.org/10.1021/acsnano.2c02016

Author Contributions

J.K. designed and performed the experimental setup, device fabrication, materials and device characterizations, data analysis, and manuscript writing. J.J. performed multiphysics simulation, mercury sensing experiments, and manuscript writing. C.W. performed the device fabrication and characterization. G.T.C. performed the device fabrication, data analysis, and manuscript writing. J.P. led the project and participated in experimental design, data acquisition, and analysis, discussions, and manuscript writing. The manuscript was written based on the contributions of all the authors. All the authors have approved the final version of the manuscript

Notes

The authors declare no competing financial interest.

ACKNOWLEDGMENTS

This work was supported by a National Research Foundation of Korea (NRF) grant funded by the Korean Government (MSIP) (2020R1A2C2009093, 2020R1A4A2002728) and by the Korea Environmental Industry & Technology Institute (KEITI) through its Ecological Imitation-Based Environmental Pollution Management Technology Development Project funded by the Korea Ministry of Environment (MOE) (2019002790007).

REFERENCES

(1) Huang, X.; Kong, X.-Y.; Wen, L.; Jiang, L. Bioinspired Ionic Diodes: From Unipolar to Bipolar. *Adv. Funct. Mater.* **2018**, *28* (49), 1801079.

(2) Cheng, L. J.; Guo, L. J. Nanofluidic diodes. *Chem. Soc. Rev.* **2010**, *39* (3), 923–938.

(3) Zhang, Z.; Wen, L.; Jiang, L. Bioinspired smart asymmetric nanochannel membranes. *Chem. Soc. Rev.* **2018**, *47* (2), 322–356.

(4) Zhang, Z.; Kong, X. Y.; Xiao, K.; Liu, Q.; Xie, G.; Li, P.; Ma, J.; Tian, Y.; Wen, L.; Jiang, L. Engineered Asymmetric Heterogeneous Membrane: A Concentration-Gradient-Driven Energy Harvesting Device. *J. Am. Chem. Soc.* **2015**, *137* (46), 14765–72.

(5) Wang, C.; Choi, E.; Park, J. High-voltage nanofluidic energy generator based on ion-concentration-gradients mimicking electric eels. *Nano Energy* **2018**, *43*, 291–299.

(6) Kim, S. J.; Ko, S. H.; Kang, K. H.; Han, J. Direct seawater desalination by ion concentration polarization. *Nat. Nanotechnol* **2010**, *5* (4), 297–301.

(7) Lin, L.; Yan, J.; Li, J. Small-Molecule Triggered Cascade Enzymatic Catalysis in Hour-Glass Shaped Nanochannel Reactor for Glucose Monitoring. *Anal. Chem.* **2014**, *86* (21), 10546–10551.

(8) Vlassiouk, I.; Kozel, T. R.; Siwy, Z. S. Biosensing with Nanofluidic Diodes. *J. Am. Chem. Soc.* **2009**, *131* (23), 8211–8220.

(9) Li, Z.-Q.; Wang, Y.; Wu, Z.-Q.; Wu, M.-Y.; Xia, X.-H. Bioinspired Multivalent Ion Responsive Nanopore with Ultrahigh Ion Current Rectification. *J. Phys. Chem. C* **2019**, *123* (22), 13687–13692.

(10) Nguyen, G.; Vlassiouk, I.; Siwy, Z. S. Comparison of bipolar and unipolar ionic diodes. *Nanotechnology* **2010**, *21* (26), 265301.

(11) Vlassiouk, I.; Siwy, Z. S. Nanofluidic Diode. *Nano Lett.* **2007**, *7* (3), 552–556.

(12) Xiao, K.; Xie, G.; Zhang, Z.; Kong, X.-Y.; Liu, Q.; Li, P.; Wen, L.; Jiang, L. Enhanced Stability and Controllability of an Ionic Diode Based on Funnel-Shaped Nanochannels with an Extended Critical Region. *Adv. Mater.* **2016**, *28* (17), 3345−3350.
(13) Siwy, Z.; Kosińska, I. D.; Fuliński, A.; Martin, C. R. Asymmetric Diffusion through Synthetic Nanopores. *Phys. Rev. Lett.* **2005**, *94* (4). DOI: 10.1103/PhysRevLett.94.048102
(14) Lin, C.-Y.; Yeh, L.-H.; Siwy, Z. S. Voltage-Induced Modulation of Ionic Concentrations and Ion Current Rectification in Mesopores with Highly Charged Pore Walls. *J. Phys. Chem. Lett.* **2018**, *9* (2), 393−398.
(15) Nguyen, Q. H.; Ali, M.; Nasir, S.; Ensinger, W. Transport properties of track-etched membranes having variable effective pore-lengths. *Nanotechnology* **2015**, *26* (48), 485502−485502.
(16) Xiao, K.; Chen, L.; Zhang, Z.; Xie, G.; Li, P.; Kong, X.-Y.; Wen, L.; Jiang, L. A Tunable Ionic Diode Based on a Biomimetic Structure-Tailorable Nanochannel. *Angew. Chem., Int. Ed.* **2017**, *56* (28), 8168−8172.
(17) Kong, Y.; Fan, X.; Zhang, M.; Hou, X.; Liu, Z.; Zhai, J.; Jiang, L. Nanofluidic Diode Based on Branched Alumina Nanochannels with Tunable Ionic Rectification. *ACS Appl. Mater. Interfaces* **2013**, *5* (16), 7931−7936.
(18) Choi, E.; Kwon, K.; Kim, D.; Park, J. Tunable reverse electrodialysis microplatform with geometrically controlled self-assembled nanoparticle network. *Lab Chip* **2015**, *15* (1), 168−178.
(19) Choi, E.; Kwon, K.; Kim, D.; Park, J. An electrokinetic study on tunable 3D nanochannel networks constructed by spatially controlled nanoparticle assembly. *Lab Chip* **2015**, *15* (2), 512−523.
(20) Choi, E.; Kwon, K.; Lee, S. J.; Kim, D.; Park, J. Non-equilibrium electrokinetic micromixer with 3D nanochannel networks. *Lab Chip* **2015**, *15* (8), 1794−1798.
(21) Choi, E.; Wang, C.; Chang, G. T.; Park, J. High Current Ionic Diode Using Homogeneously Charged Asymmetric Nanochannel Network Membrane. *Nano Lett.* **2016**, *16* (4), 2189−97.
(22) Syed, A.; Mangano, L.; Mao, P.; Han, J.; Song, Y. A. Creating sub-50 nm nanofluidic junctions in a PDMS microchip via self-assembly process of colloidal silica beads for electrokinetic concentration of biomolecules. *Lab Chip* **2014**, *14* (23), 4455−60.
(23) Lee, J.; Lee, K.; Wang, C.; Ha, D.; Kim, G. H.; Park, J.; Kim, T. Combined Effects of Zeta-potential and Temperature of Nanopores on Diffusioosmotic Ion Transport. *Anal. Chem.* **2021**, *93* (42), 14169−14177.
(24) Lan, W. J.; Holden, D. A.; Zhang, B.; White, H. S. Nanoparticle Transport in Conical-Shaped Nanopores. *Anal. Chem.* **2011**, *83* (10), 3840−3847.
(25) Qiu, Y.; Vlassiouk, I.; Hinkle, P.; Toimil-Molares, M. E.; Levine, A. J.; Siwy, Z. S. Role of Particle Focusing in Resistive-Pulse Technique: Direction-Dependent Velocity in Micropores. *ACS Nano* **2016**, *10* (3), 3509−3517.
(26) Ali, M.; Yameen, B.; Neumann, R.; Ensinger, W.; Knoll, W.; Azzaroni, O. Biosensing and Supramolecular Bioconjugation in Single Conical Polymer Nanochannels. Facile Incorporation of Biorecognition Elements into Nanoconfined Geometries. *J. Am. Chem. Soc.* **2008**, *130* (48), 16351−16357.
(27) Daiguji, H.; Oka, Y.; Shirono, K. Nanofluidic Diode and Bipolar Transistor. *Nano Lett.* **2005**, *5* (11), 2274.
(28) Pu, Q.; Yun, J.; Temkin, H.; Liu, S. Ion-enrichment and ion-depletion effect of nanochannel structures. *Nano Lett.* **2004**, *4* (6), 1099−1103.
(29) Zeng, Y.; Harrison, D. J. Self-assembled colloidal arrays as three-dimensional nanofluidic sieves for separation of biomolecules on microchips. *Anal. Chem.* **2007**, *79* (6), 2289−2295.
(30) Kim, S. J.; Ko, S. H.; Kwak, R.; Posner, J. D.; Kang, K. H.; Han, J. Multi-vortical flow inducing electrokinetic instability in ion concentration polarization layer. *Nanoscale* **2012**, *4* (23), 7406−10.
(31) Zhiyue, M.; Xichen, Y.; Li, R.; Yang, Y.; Huicheng, F.; Peng, S. Recent advances in paper-based preconcentrators by utilizing ion concentration polarization. *Electrophoresis* **2021**, *42* (12−13), 1340−1351.
(32) Gholinejad, M.; Jabari Moghadam, A.; Phan, D. T.; Miri, A. K.; Mousavi Shaegh, S. A. Design and application of ion concentration polarization for preconcentrating charged analytes. *Phys. Fluids* **2021**, *33* (5), 051301.
(33) Huang, K. D.; Yang, R. J. Formation of ionic depletion/enrichment zones in a hybrid micro-/nano-channel. *Microfluid Nanofluid* **2008**, *5* (5), 631−638.
(34) Kim, S. J.; Han, J. Y. Self-sealed vertical polymeric nanoporous-junctions for high-throughput nanofluidic applications. *Anal. Chem.* **2008**, *80* (9), 3507−3511.
(35) De Acha, N.; Elosúa, C.; Corres, J.; Arregui, F. Fluorescent Sensors for the Detection of Heavy Metal Ions in Aqueous Media. *Sensors* **2019**, *19* (3), 599.
(36) Chung, C. H.; Kim, J. H.; Jung, J.; Chung, B. H. Nuclease-resistant DNA aptamer on gold nanoparticles for the simultaneous detection of Pb2+ and Hg2+ in human serum. *Biosens. Bioelectron.* **2013**, *41*, 827−832.
(37) Li, S. X.; Guan, W.; Weiner, B.; Reed, M. A. Direct Observation of Charge Inversion in Divalent Nanofluidic Devices. *Nano Lett.* **2015**, *15* (8), 5046−51.
(38) He, Y.; Gillespie, D.; Boda, D.; Vlassiouk, I.; Eisenberg, R. S.; Siwy, Z. S. Tuning transport properties of nanofluidic devices with local charge inversion. *J. Am. Chem. Soc.* **2009**, *131* (14), 5194−202.
(39) Patil, S. K.; Das, D. A nanomolar detection of mercury(II) ion by a chemodosimetric rhodamine-based sensor in an aqueous medium: Potential applications in real water samples and as paper strips. *Spectrochim Acta A Mol. Biomol Spectrosc* **2019**, *210*, 44−51.
(40) Lam, P.; Wynne, K. J.; Wnek, G. E. Surface-Tension-Confined Microfluidics. *Langmuir* **2002**, *18* (3), 948−951.
(41) Sorsak, E.; Volmajer Valh, J.; Korent Urek, S.; Lobnik, A. Design and Investigation of Optical Properties of N-(Rhodamine-B)-Lactam-Ethylenediamine (RhB-EDA) Fluorescent Probe. *Sensors (Basel)* **2018**, *18* (4), 1201.
(42) Singh, K. P. Ion current rectification influenced by length and location of surface charge in fluidic unipolar conical nanopores. *Sens. Actuators, B* **2016**, *230*, 493−500.
(43) Cai, J.; He, Q.; Song, L.; Han, L.; Liu, B.; Zhao, Y.; Chen, W.; Zhan, D. Ion Current Rectification Behavior of Conical Nanopores Filled with Spatially Distributed Fixed Charges. *J. Phys. Chem. C* **2019**, *123* (43), 26299−26308.
(44) Mathwig, K.; Aaronson, B. D. B.; Marken, F. Ionic Transport in Microhole Fluidic Diodes Based on Asymmetric Ionomer Film Deposits. *ChemElectroChem.* **2018**, *5* (6), 897−901.
(45) Cervera, J.; Schiedt, B.; Neumann, R.; Mafe, S.; Ramirez, P. Ionic conduction, rectification, and selectivity in single conical nanopores. *J. Chem. Phys.* **2006**, *124* (10), 104706.
(46) Zhao, C.; Zhang, H.; Hou, J.; Ou, R.; Zhu, Y.; Li, X.; Jiang, L.; Wang, H. Effect of Anion Species on Ion Current Rectification Properties of Positively Charged Nanochannels. *ACS Appl. Mater. Interfaces* **2020**, *12* (25), 28915−28922.
(47) Liu, Q.; Liu, Y.; Lu, B.; Wang, Y.; Xu, Y.; Zhai, J.; Fan, X. A high rectification ratio nanofluidic diode induced by an "ion pool. *RSC Adv.* **2020**, *10* (13), 7377−7383.
(48) Liu, F. F.; Guo, Y. C.; Wang, W.; Chen, Y. M.; Wang, C. In situ synthesis of a MOFs/PAA hybrid with ultrahigh ionic current rectification. *Nanoscale* **2020**, *12* (22), 11899−11907.